Materials Research Express

PAPER • OPEN ACCESS

Development of structural colored TiO_2 thin films by varied etching solutions

To cite this article: Ozan Yilmaz *et al* 2023 *Mater. Res. Express* **10** 056401

View the article online for updates and enhancements.

You may also like

- Multifunctional soft stretchable strain sensor for complementary optical and electrical sensing of fatigue cracks
Han Liu, Matthias Kollosche, Simon Laflamme et al.
- Study of Structural Colors of Anodic Alumina Thin Films Prepared by a Point Electrode
Shumin Yang, Wei Han, Haitao Li et al.
- Fully wireless pressure sensor based on endoscopy images
Yusaku Maeda, Hirohito Mori, Tomoaki Nakagawa et al.

This content was downloaded from IP address 150.244.101.138 on 11/07/2023 at 11:09

Materials Research Express

PAPER

Development of structural colored TiO_2 thin films by varied etching solutions

Ozan Yilmaz[1,2], **Ramazan Dalmis**[2,*], **Tuncay Dikici**[3,4] and **M Faruk Ebeoglugil**[1,2]

[1] Dokuz Eylul University, The Graduate School of Natural and Applied Sciences, Buca, 35390, Izmir, Turkey
[2] Dokuz Eylul University, Department of Metallurgical and Materials Engineering, Buca, 35390, Izmir, Turkey
[3] Dokuz Eylul University, Center for Fabrication and Applications of Electronic Materials (EMUM), Buca, 35390, Izmir, Turkey
[4] Dokuz Eylul University, Torbalı Vocational School, Welding Technology, Torbali, Turkey
[*] Author to whom any correspondence should be addressed.

E-mail: ramazan.dalmis@deu.edu.tr

Keywords: self-cleaning, structural color, fabry-perot, photonic crystal, photocatalytic, anodization

OPEN ACCESS

RECEIVED
5 February 2023

REVISED
6 April 2023

ACCEPTED FOR PUBLICATION
26 April 2023

PUBLISHED
5 May 2023

Original content from this work may be used under the terms of the Creative Commons Attribution 4.0 licence.

Any further distribution of this work must maintain attribution to the author(s) and the title of the work, journal citation and DOI.

Abstract

Currently, one of the most important problems is water scarcity due to increasing population and environmental factors. Humankind can overcome this problem by recycling polluted water. The structural colors obtained from photonic crystal structures draw attention with fadeless bright color, combined with low toxicity and eco-friendliness. In this study, different etching/anodizing processes were applied to obtain Fabry-Perot and Photonic Crystal Ti-TiO_2 structures. Structural colors owing to the morphology of the anatase phase on the surface of the samples etched with hydrochloric, sulfuric, and hydrofluoric acid-based solutions were obtained. The structural color of the formation on the titanium surfaces is related to the Fabry-Perot structures, while variations were correlated with Photonic Crystal surface morphologies. Because the high reflectance values contributed to the structural color formation, the photocatalytic efficiency of the samples etched with acid-based solutions was found to be lower than the samples etched with basic sodium and potassium hydroxide solutions. High-efficiency structural color reactors can be obtained by shifting the reflected wavelength range from the absorption wavelength range of the pollution material.

1. Introduction

Due to global warming and increasing water pollution, purifying wastewater has become critical [1–3]. Photocatalytic water treatment is a green treatment for purifying wastewater contaminated by dyes, bacteria, viruses, heavy metals, estrogens, chlorinated hydrocarbons, dioxins, and pharmaceuticals [4–6]. Photocatalytic treatment is a very cost-effective process due to the sole input of solar energy [4]. Disposal of environmental contaminants is carried out by the oxidation/reduction reactions of valence band holes and conduction band electrons in semiconductor photocatalysts [4]. TiO_2 is a very popular photocatalyst material organic substance in water by using UV light irradiation [7, 8].

A TiO_2 layer forms on the surface when the metallic Titanium is exposed to air for a while [9]. If the thickness of the TiO_2 layer exceeds about 20 nm, structural color formation due to light interferences is observed [9, 10]. Layers with different dielectric properties are required in order to provide refractions between layers and to obtain light of the same wavelength. Photonic Crystal (PC) [11–13] and Fabry-Perot (FP) [14–17] materials are popular with these characteristics. Photonic crystals have dielectric contrast arrangements in one, two, and three dimensions while Fabry-Perot systems have dielectric contrast in only one dimension. Brilliant structural colors in nature have attracted to huge scientific attention for a long time [18–21]. Structural color is obtained by the physical interactions of light including diffraction, scattering, and interference within the periodic nanostructure without any pigment [21–24]. Structural colors are observed mostly in bird and butterfly feathers and insect wings in nature [25, 26]. However, they can be obtained artificially only with photonic crystal materials. If the photonic band gap of the photonic crystal (or FP) is located in the visible wavelength range, it

© 2023 The Author(s). Published by IOP Publishing Ltd

Table 1. Sample abbreviations according to the etching chemical types, etching time, and anodization process.

Sample code	Etching chemicals	Etching time	Temperature (°C)	The anodization process
E1	$HCl+H_2SO_4$	10 min	60	—
E2	$HF+HNO_3+H_2SO_4$	10 min	60	—
E3	NaOH+D. water	24 h	60	—
E4	KOH+D. water	24 h	60	—
EA1	$HCl+H_2SO_4$	10 min	60	+
EA2	$HF+HNO_3+H_2SO_4$	10 min	60	+
EA3	NaOH+D. water	24 h	60	+
EA4	KOH+D. water	24 h	60	+

reflects colors of the related wavelength range [27]. Many applications started to appear for structural colored materials including decoration, anti-counterfeiting, color displays, and hydrophobicity [28–32]. Structural colorization will take more reputation in the future compared to the pigments consisting of chemicals due to their brilliant colors, high saturation, iridescence, not fading, low toxicity and eco-friendly properties [22, 32–35].

Recently, there have many studies on the fabrication of photonic crystals by the anodic growth/etching technique have focused on alumina PC structures from aluminum [13, 21, 27, 36–41]. For example, Kushnir *et al* produced anodic alumina coatings with iridescent structural colors by the cyclic anodization technique of aluminum [27]. They observed that increasing the anodization cycle numbers caused a blue shift and an increase in color depth [27]. In another study, Ding *et al* [42] obtained structurally colored porous iron oxide coatings by femtosecond laser application. However, there are very few studies on etching solution investigation of structural colored TiO_2 thin film properties to our knowledge. Therefore, the main aim is to reveal how different solutions affect structural color formation. In addition, a detailed analysis of the obtained colors and detailed research on how they affect the photocatalytic properties are presented. Physical, morphological, optical, and photocatalytic analysis results of the coatings were characterized.

2. Experimental procedure

2.1. Preparation of the nanostructured TiO_2 films

Titanium rods were subjected to sample preparation processes before anodizing. Firstly, pure titanium rods were cut as 25 mm in diameter and 5 mm in thickness. Sanding was applied using 120–2000 sandpapers. Finally, polishing and cleaning processes were applied. To remove the oxide layers on the surface that may have formed just before the etching and anodization process, a short pre-treatment process in nitric acid (HNO_3) and hydrofluoric acid (HF) bath was performed. Thus, all substrates for chemical and electrochemical procedures were ready. Hydrochloric acid (HCl), sulfuric acid (H_2SO_4), hydrofluoric acid (HF), sodium hydroxide (NaOH), and potassium hydroxide (KOH) chemicals and pure water were used to prepare etching solutions. Sample abbreviations according to the etching chemical types, etching time, and anodization process are presented in table 1. E1, E2, E3, and E4 samples were only subjected to an etching process, while AE1, AE2, AE3, and AE4 samples were both etched and anodized.

The distance between the anode and cathode was adjusted to 4–5 cm during anodization. EA1-EA4 samples were anodized in 0.05% HF solution under 20 V voltage for 30 min. After the anodization process, all samples were annealed at 450 °C for 2 h, in an air environment similar to the literature [43]. The samples were kept in a desiccator after the treatments to expose them to low humidity.

2.2. Characterization methods

Phase characterizations of the thin films were carried out by means of Rigaku D/Max-2200/PC x-ray Diffractometer in the 2θ range; thin film mode at a scan speed of 2°/min. CuK_α radiation with an energy value of 8048.3 eV was obtained at the 40 kV and 36 mA parameters. The surface morphologies of the thin films were characterized with JEOL-JSM 6060 model scanning electron microscope (SEM). However, Carl Zeiss 300VP, an SEM device with a higher magnification capacity was used to examine the surface morphologies of the E2/AE2 samples. A Thermo Scientific Evolation 600 UV-VIS Spectrophotometer was used for reflectance measurements of the coatings in the visible range between 275 nm − 800 nm wavelengths. A Nikon Eclipse ME600 model optical microscope and Zeiss Discovery V12 stereo microscope devices were used to demonstrate the structural colors of the thin films.

The photocatalytic characterizations were carried out in a reactor equipped with an exhaust fan cooling system to hold the chamber at room temperature. The photocatalytic performance of the samples was detected

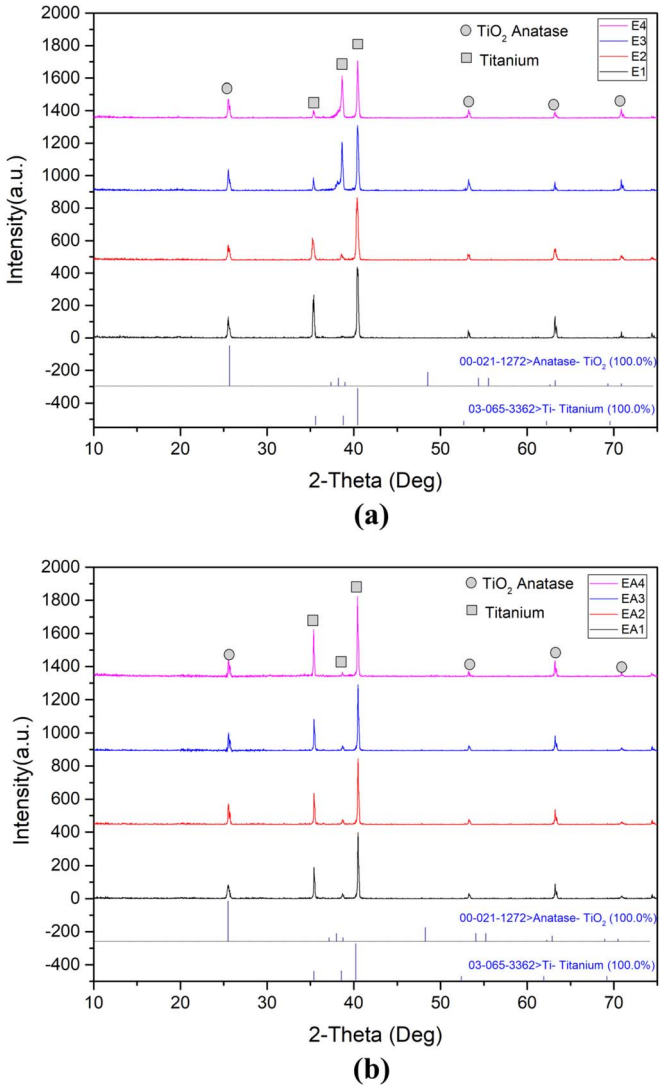

Figure 1. XRD patterns of the (a) etched and (b) anodized samples [47] after the annealing process.

according to the absorbance values of methylene blue (MB) versus the wavelength range of 500 to 800 nm in quartz beakers. For each test, samples were placed in a beaker with 30 ml of MB aqueous solution at a concentration of 10^{-5} M. The Osram Ultra Vitalux E27 light source, with 300 W and 1.9 W cm^{-2} intensity delivered UV–vis light. The UV-1240 Shimadzu spectrophotometer was used to measure the degradation of the MB solution using the characteristic absorbance peak of MB at 664 nm. Every 30 min, 5 ml suspension was taken out for measurements after precipitation of particles by centrifugation.

3. Results and discussions

3.1. Phase analysis

To determine the phases of TiO_2 films, XRD analysis was performed after annealing at 450 °C for 2 h. XRD patterns are shown in two separate groups as only etched (figure 1(a)) and anodized etched (figure 1(b)) samples. It is reasonable to interpret that the two sample groups are together, as all samples peak in the same regions. All samples have diffraction peaks at 2θ values of 24.8°, 53.5°, 62.83°, 70.55° and corresponding to the (101), (105), (204) and (215) crystal planes, respectively (see figure 1). These values are the angles and crystal planes of the crystalline Anatase phase of the TiO_2 crystal structure (JCPDS Card No: 12–1272) [44]. The peaks are found at $2\theta = 35.3°$, 38.6° and 40.3° matching the Ti (JCPDS # 03–065–3362) crystalline planes (100), (002), (101) [45] comes from the substrate. Rutile and brookite phases were not found in any sample in either group [46]. Some differences in intensity were observed between the etched and etched/anodized samples.

The main reason for the difference in intensity between the etched and etched/anodized samples is the differences in the oxidation mechanism. With the anodization process, chemical reactions and electrical

Table 2. Elemental composition results according to the EDS analysis.

Samples	Mole concentration (%) of the components		
	Ti	O	C
E1	51.96	30.98	17.06
E2	47.80	36.16	16.04
E3	41.86	38.51	19.63
E4	44.65	42.43	12.92
EA1	50.77	34.66	14.57
EA2	44.75	36.16	19.09
EA3	41.56	38.63	19.81
EA4	43.81	45.48	10.71

reactions occur in succession. The pH value, morphology, and oxidation reactions of the etching solutions may be the cause of these intensity variations [48]. Different etching solutions (E1, E2, E3, and E4) had different pH values. Therefore, the absorption of O_2 ions in the oxidation phenomenon is affected, and so is the crystallinity intensity. For acidic concentrations, polarization increases as the pH value decreases (<3), while for base concentrations the pH value increases (>10) polarization increases. This situation leads to the formation of differentiation in the peak intensities in the XRD patterns [49]. However, the TiO_2 crystallization without thermal treatment needs a longer time to approach. With the anodization process, the oxidation transfer can be out easily due to the voltage thermal effect. So all these anodized samples were stabilized at the same intensity values after the anodization process [50]. The short process time facilitated the completion of the crystallization cycle and this paved the way for a stable intensity [46].

The elemental composition results of the samples are presented in table 2, to provide more in-depth information about the surface composition. As shown in table 2, all samples consist of Ti, O, and C elements. It can be observed that Ti and O, which have the highest element ratios, are between 51.96%-41.56% and 45.48%-30.67% values, respectively. Carbon exists on all sample surfaces because it has been absorbed from the environment and cannot be eliminated from the surface [51]. A traditional effective depth of EDS is just a few micrometers. When the sample surface is open to the air, the surface is easily exposed to carbon. However, the carbon ratio is around 19%, it is not enough to say that the environment alone causes it. Another reason might be production with sol-gel. Excess carbon might be left during the removal of organic structures from the body by the calcination process.

3.2. Surface morphology

The surface morphology of the samples after etching and anodization procedures have great importance for surface properties. General and close SEM images of the samples exposed to surface treatments are presented in figure 2. The SEM images of the E1 sample etched with HCl-H_2SO_4, an acidic solution, subsequently anodized AE1 sample can be viewed in figures 2(a) and (b), respectively. This caused abrasions on the surfaces of both samples, as expected from the acidic solution [52]. It can be seen that the obtained indentation-protrusion morphology is similar to the study that was etched with the same solution [53]. It can be observed that the grain boundaries started to appear in the microstructures of both samples, but they could not provide grain separation very clearly. The surface morphology of the E1 sample given in figure 2(a) is one of the most striking results. Regular indentations and protrusions are observed on the E1 sample surface by the effect of chemical abrasives. This structure, which is evident from the close view, can be compared to the morphology of the Morpho butterfly wings with regular indentations and protrusions [54]. These regular indentations and protrusions trigger the formation of structural color due to the dielectric contrast [54–56]. It is observed that pores grow more on the surface of the AE1 sample (see figure 2(b)), which is the anodized form of the E1 sample. The pitting on the EA1 sample surface does not display a perfect order. The surface morphologies of the E2 and AE2 samples etched with HF+HNO_3+H_2SO_4 and then anodized, are presented in figures 2(c) and (d), respectively. As can be understood from the close and general images, the grain boundaries are quite eroded and the grains have become distinct. The presence of nanopores is striking in the detailed images. The HF+HNO_3 chemicals added to the H_2SO_4 caused erode the high-energy grain boundaries much more and caused the micro-pores to turn into nanopores.

SEM images of the E3 etched by NaOH solution and then anodized AE3 sample are given in figures 2(e) and (f), respectively. A three-dimensional porous morphology is observed on the surface of the E3 sample (see figure 2(e)) similar to the previous studies [57, 58]. We observe that the pore sizes are in both micro- and

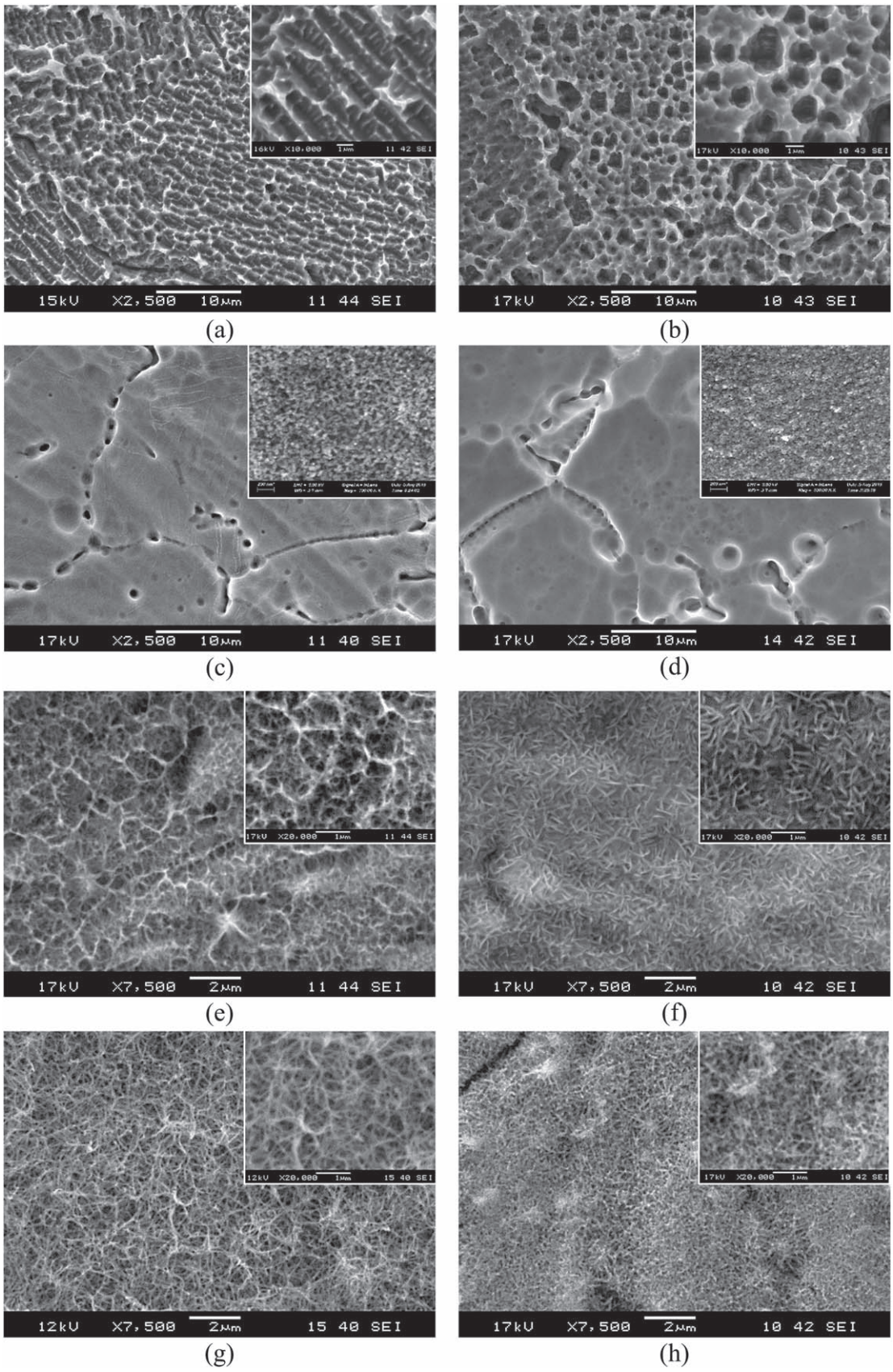

Figure 2. SEM images of the etched (a) E1,(c) E2, (e) E3, (g) E4 and etched/anodized (b) EA1, (d) EA2, (f) EA3, (h) EA4 samples [47].

nanodimensions. After the anodization procedure, major differences occurred in the surface morphology. It is seen that the pores are mostly closed, and the flake morphology is formed after the anodization procedure (see figure 2(f)). The surface of the E4 sample etched with KOH is so abraded that the surface has a three-dimensional

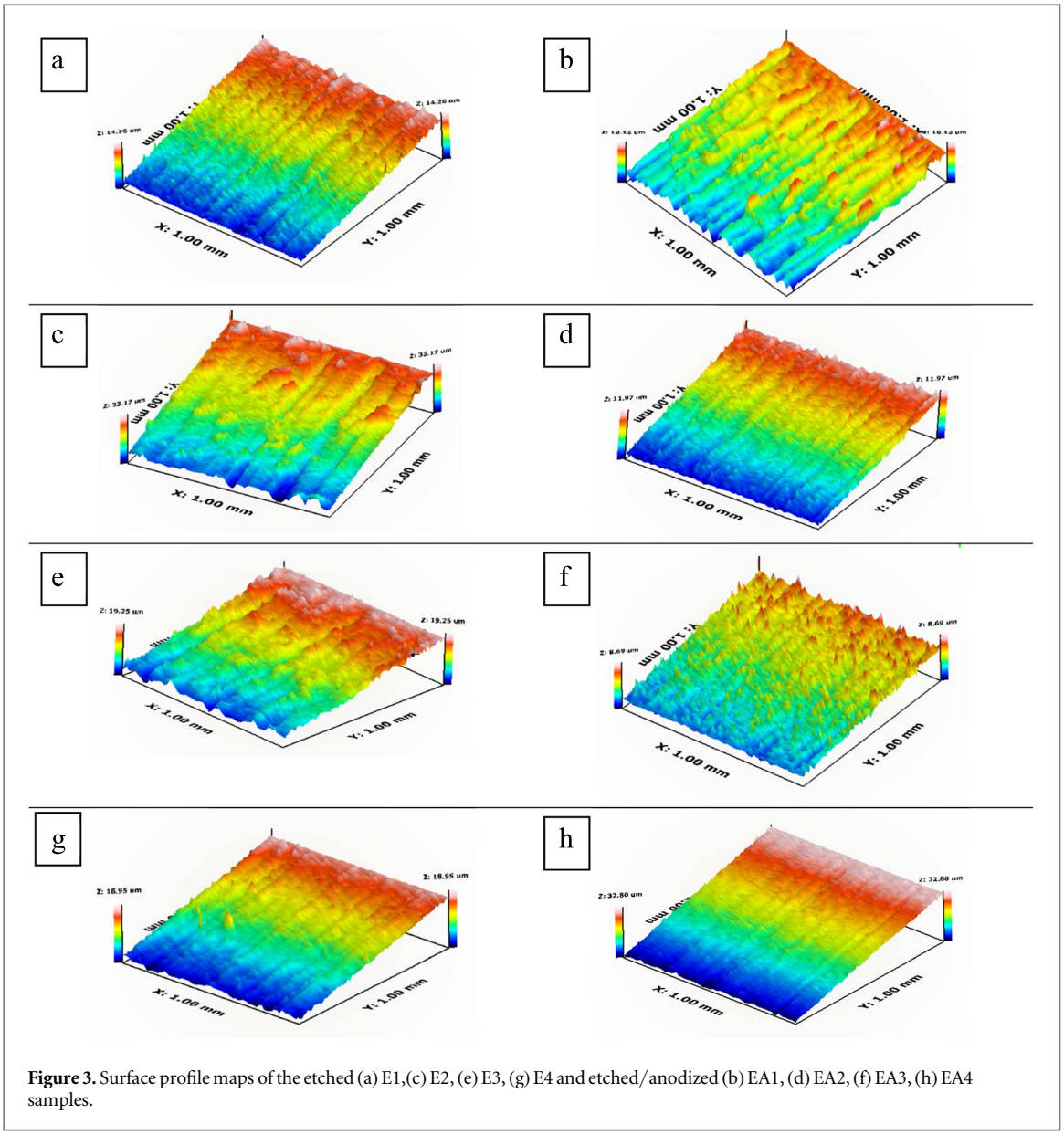

Figure 3. Surface profile maps of the etched (a) E1,(c) E2, (e) E3, (g) E4 and etched/anodized (b) EA1, (d) EA2, (f) EA3, (h) EA4 samples.

reticulated morphology (see figure 2(g)) in accordance with the literature [59]. This linked nanofiber morphology has given the surface a very porous character. The samples obtained with the fourth solution with macro and nanofiber morphology have the highest surface area, while the samples obtained with the first solution, which only creates micro indentations-protrusions have the lowest surface area (see figure 2). It is quite consistent that the fourth solution samples with nanofiber surface morphology with high surface area exhibit the highest efficiency, while the samples abraded with the first solution, which creates indentations and microporous on the surface, show the lowest yields according to the photocatalytic results. Some changes occurred in the morphology of the AE4 sample (see figure 2(h)) after anodization procedure, similar to the AE3 sample. Most pores due to fibrous morphology were turned into a more micro-porous structure after the anodization process.

Surface profile maps obtained by scanning from 1mm × 1mm areas of etched and etched/anodized samples are shown in figure 3. It can be observed that there is periodic indentation and protrusion morphology, especially at etched with first and second solutions (see figures 3(a)–(d)) according to the general view. The created morphology is very similar to the morphologies observed in the wings of the structurally colored butterflies, including *M.sulkowskyi*, *A.m.eudaemon*, *O.p.poseidon*, and *P.sesostris* species [60]. They think that the periodic ridges lead to the anisotropic effective refractive indices in the parallel and perpendicular grating orientations led to a phase difference between two different component-polarized lights [60]. If this difference is in the visible wavelength range, the structural color formation is observed. We assume the color formation on the anodized Ti surfaces similar to their explanation of structural color formation. By using the surface maps, the average surface roughness of the samples were calculated. Average surface roughness values of the E1, E2, E3, E4

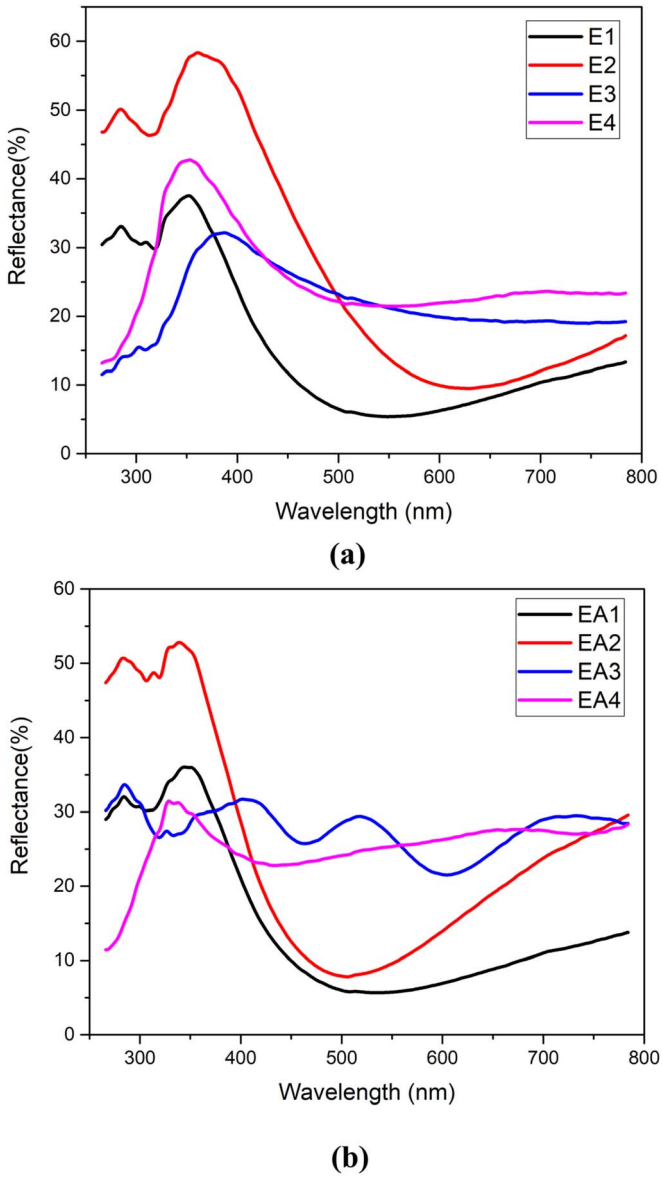

Figure 4. Reflectance spectra of the (a) etched and (b) etched-anodized samples in the UV-Visible range.

samples are determined as 2.73 μm, 5.53 μm, 2.31 μm, 3.60 μm, respectively; the EA1, EA2, EA3, EA4 samples are found as 1.43 μm, 3.75 μm, 1.15 μm, and 3.49 μm, respectively. As a result, the anodizing process reduced the roughness values of the samples.

3.3. Optical properties

3.3.1. UV-vis spectrum

Reflectance spectra of the etched and etched-anodized samples in the UV-Visible range are presented in figures 4(a) and (b), respectively. Reflection data from the UV-vis region is of great importance for the interpretation of the photonic band gap and photocatalytic performance. While the samples etched with the second solution had the highest reflectance values, the lowest reflectance values were observed in the samples etched with the fourth solution. Structural colorization on the Ti substrates after anodization is attributed to the reflect a coherent visible wavelength by the interference between the TiO_2 layer and Titanium metal [10, 11, 61]. Both the Photonic Crystal and Fabry-Perot definitions cover this coherent scattering. The structural color formation is observed when the light diffracted between layers with different dielectric properties reaches the same frequency in the visible wavelength. The higher the dielectric contrast between the scattering layers, the more vivid structural color is obtained with narrower PBG. It can be seen that the E1 and E4 samples showed peaks at approximately 350 nm, the E2 sample at 361 nm and the E3 sample at 387 nm according to figure 4(a). These values are related to the pseudophotonic bandgap (pPBG) values of the produced samples and therefore

the colors they exhibit [24, 62, 63]. Hence, violet and blue colors will be dominant on the surfaces of the etched samples.

While the highest reflectance value belongs to the E2 sample (58%), the lowest value belongs to the E3 sample (32%). It is striking that the E2 sample with nanopores gives the highest reflectance value. The pPBG term is preferred since the intensity of the reflectance peaks is not 100%. This may be due to changes in microstructure not being in perfect order. The reflectance curves of the E3 and E4 samples show a similar character with a sharp peak and a shoulder evolving in the visible wavelength range. The structural color of titanium surfaces is explained by Fabry-Perot structures as mentioned above. In these systems, the observed color is strongly affected by the number of layers, layer thickness, the refractive index of the media, and the angle of incidence light, which are the variables in Snell's law [10, 11, 61]. There is a critical difference in the reflectance curves of the E1 and E2 samples compared to the E3 and E4 samples, which is displaying a reflectance peak in the ultraviolet region. To explain the color variation, it would be correct to evaluate the morphologies of the samples from the SEM images. This situation is thought to be due to more regular surface morphologies. Regular indentations-protrusions and porous morphologies in E1/EA1 and E2/EA2 samples (figure 2) increase coherent scatterings. Meaning, PC surfaces help FP structures for structural colorization.

The reflectance spectra of etched and anodized samples (EA) are similar to those of just etched samples (E). According to figure 4(b), The AE1, AE2 and AE4 samples exhibit peaks at approximately 395 nm, 390 nm and 325 nm, respectively. The reflectance values of AE1 and AE2 increased again after 500 nm. The AE3 sample differs from other samples with its small reflectance peaks of 285 nm, 404 nm, 517 nm and 706 nm. Moreover, the AE4 sample stands out as the only sample that does not indicate a reflectance peak in the UV region. The reflection of the high-energy UV light from the sample surface may mean energy lose used in photocatalytic reactions. Additionally, the stability of EA3 and EA4 samples at reflectance values of about 30% in the visible wavelength range indicates that no color can occur on their surface. When figures 4(a) and (b) are examined together, it can be seen that the anodization process causes some changes in the reflectance behavior of the etched samples. The most obvious one of these changes was the shifting of the reflectance peak values of the etched samples toward the lower wavelengths (blue shift) by the anodization process. Additionally, the anodization process decreased reflectance peaks, albeit in insignificant amounts.

3.3.2. Stereo and optical microscopic images

Stereo and optical microscope images of the produced samples are gathered in figure 5, to observe the structural color formation in and their suitability for microstructure examinations. structural color formation could be easily interpreted from stereomicroscope images given in the upper right part of the optical microscope images (figure 5), in smaller sizes. This is observed from the optical images (figure 5) that purple and blue colors are dominant on the sample surfaces that show reflectance peaks at 300 to 425 nm and extend up to 550 nm (see figure 5) mentioned in the UV-Vis spectrum part. Generally, it was observed that purple, blue, and orange colors were formed on the etched and anodized sample surfaces etched by the first and second solutions and that these colors did not occur on the samples treated with the third and fourth solutions. This is strongly related to the surface morphologies of the samples. E1 sample surface similar to the one-dimensional (1D) photonic crystal surface of the Morpho butterfly [54, 56], while E2, AE1, EA2 sample surfaces are similar to two-dimensional (2D) photonic crystal surfaces with nanomicro pores [64].

We observe that purple is dominant in the general image of the E1 sample, while purple and orange colors are dominant in optical microscope images according to figure 5(a). As mentioned in the reflectance results, the E1 and AE1 samples exhibited high reflectance values at the purple and blue wavelength regions. Therefore, these structural colorations were consistent with the reflectance results and became darker with a blue shift after anodization. The decrease in the intensity of the purple wavelength region and the increase in the orange wavelength region on the reflectance curve of the AE1 sample (see figure 4(b)) contributed to the predominance of the orange in the microstructure (figure 5(b)). The microstructure of the E2 sample etched with the second solution is the most striking structure among the optical microscope images. The grain boundaries of the anatase structure are clearly visible in the microstructure image of the E2 sample, as can be observed in figure 5(c). The microstructure image of the E2 sample can be used for microstructure examinations colored purple and orange structural colors. Thus, the second etching solution can be used as an etching solution for microstructure investigations of titanium. After the anodization process, the blue became dominant on the surface of the AE2 sample (figure 5(d)). The increase in the efficiency of the reflectance peak by the reflectance curve of the AE2 sample decreasing to lower levels at 500 nm (see figure 4(b)) may have caused the domination blue. A slight green formation is also noticeable on the E3 sample surface etched by the third solution (figure 5(e)). Since the sample E3, which currently exhibits a very low reflectance peak, transformed some weak peaks close to each other (see figure 4(a)) after anodization (AE3), no structural color formation was observed on the surface (figure 5(f)). The general appearance of the AE3 sample in figure 5(f), a slight blue formation can be associated with the weak peak approximately 404–455 nm (figure 4(b)). The fact that no color formation is observed on the surfaces of the E4

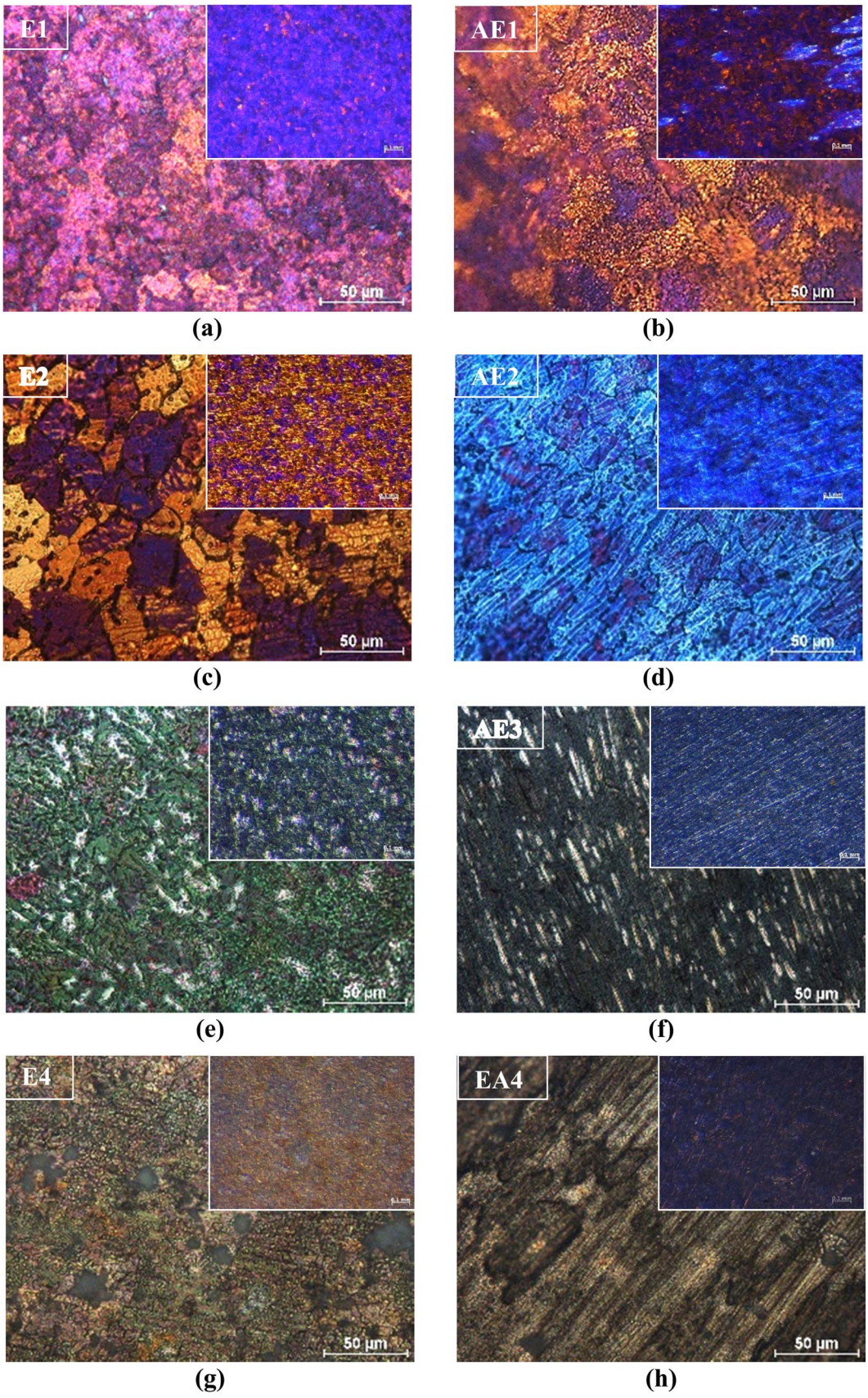

Figure 5. Optic and stereo microscope images of the just etched (a) E1, (c) E2, (e) E3, (g) E4 samples and etched-anodized (b) AE1, (d) AE2, (f) AE3, (h) AE4 samples. Stereomicroscope images are located in the upper right part of the optical microscope images, in smaller.

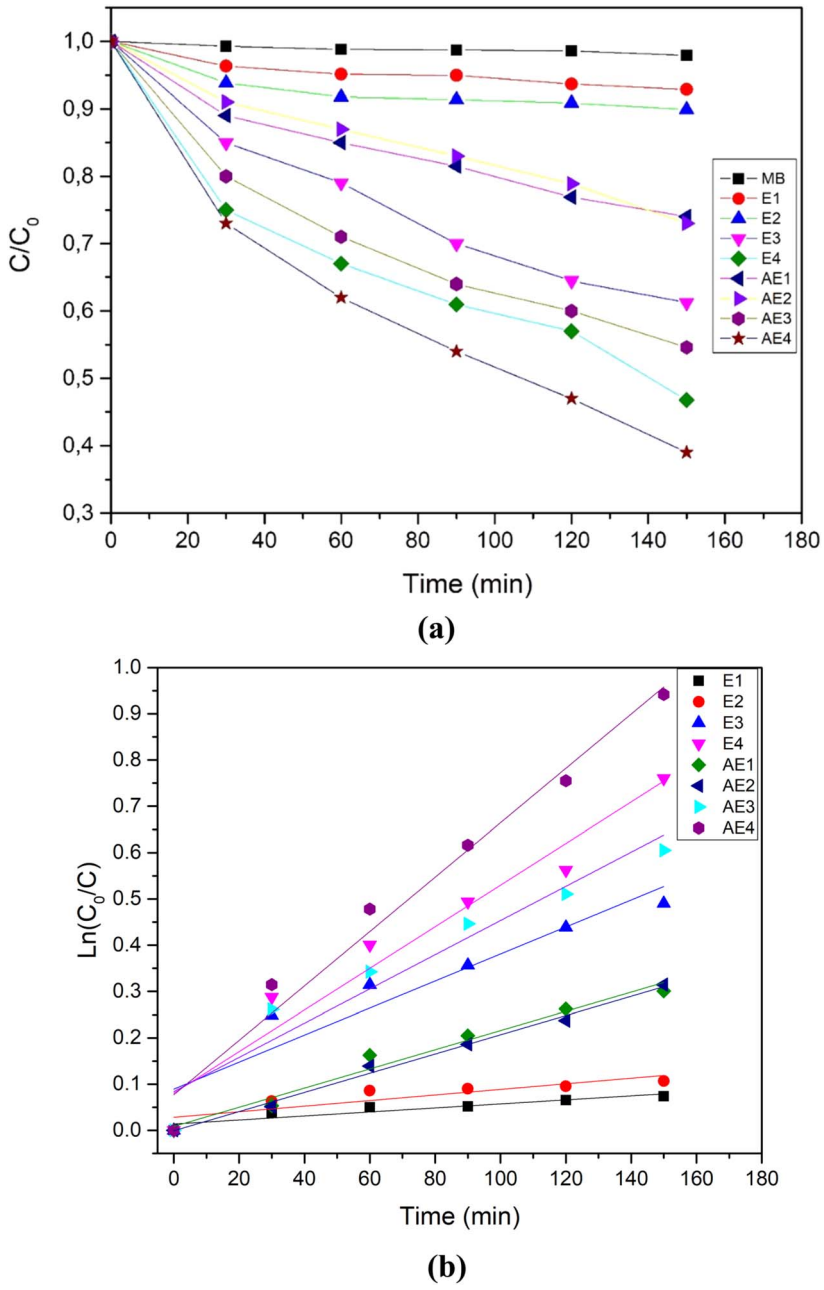

Figure 6. (a) Photodegradation efficiency curves with MB and (b) kinetic constants of the TiO_2 films.

and AE4 samples (see figures 5(g) and (h)) prepared with the fourth solution can be attributed to the concentration of reflectance peaks in the UV region and not extend too much into the visible region.

3.4. Photocatalytic degradation and kinetic mechanism

The maximum absorbance spectrum was obtained in methylene blue and a wavelength of 664 nm to obtain photocatalytic results. Figure 6(a) shows the time-dependent dissolution performance of MB-resolved TiO_2 films. Absorbance values of etched and anodized samples were obtained under UV light. Previously, it was kept in the MB solution in a dark environment, and the degradation obtained was negligible. It can be observed that there is a big variation in the photocatalytic performance of the samples (figure 6). It could be due to the different pH values of different etching concentrations lead to differentiation in morphology and optical properties. In acidic solutions, if the pH value is less than 3, it has a negative effect since polarization begins and affects the absorption of O_2 ions in oxidation. The basic concentration also affects the absorption of O_2 molecules of the OH^- radical group with an increase in pH (pH $>$ 10) [49].

Photocatalytic kinetic studies of etched and etched/anodized TiO_2 films were also examined to understand the kinetics during the degradation phase. The formula of the kinetic mechanism shown in figure 6(b) is

explained as follows:

$$\ln\left(\frac{C_o}{C}\right) = kt \tag{1}$$

In figure 6(b), the photocatalytic degradation percentage is seen in the MB solution of the samples. The photocatalytic kinetics were determined according to the formula ln (C_0/C). C_0 corresponds to the original concentration, while C represents the comparative concentration. The symbol of k is a degradation constant [49].

How the step-by-step degradation mechanism occurs place for methylene blue is explained below [65, 66];

$$TiO_2 + hv \rightarrow TiO_2\,(e^- + h^+) \tag{2}$$

$$Dye + TiO_2(h^+) \rightarrow Oxidation\ process \tag{3}$$

$$TiO_2(h^+) + H_2O \rightarrow OH\cdot + H^+ + TiO_2 \tag{4}$$

$$TiO_2(h^+) + OH^- \rightarrow TiO_2 + OH\cdot \tag{5}$$

$$Dye + TiO_2(e^-) \rightarrow Reduction\ Process \tag{6}$$

$$TiO_2(e^-) + O_2 \rightarrow TiO_2 + O_2^{\cdot -} \tag{7}$$

$$O_2^{\cdot -} + H^+ \rightarrow HO_2^{\cdot} \tag{8}$$

$$HO_2^{\cdot} + HO_2^{\cdot} \rightarrow H_2O_2 + O_2 \tag{9}$$

$$H_2O_2 + O_2^{\cdot -} \rightarrow OH\cdot + OH^- + O_2 \tag{10}$$

$$Dye + OH\cdot \rightarrow Degradation\ Products \tag{11}$$

The way degradation mechanism progresses; the first absorption of light, then excited hole and electron separation, next movement of photo-generated charge carriers toward the surface of the catalyst, and at last redox reaction through adsorbed reactants [67]. As can be seen from equation (2), light energy (hv) is critical for all relevant reactions to occur. To use maximum energy, high-energy short wavelengths such as UV, must be harvested well. However, if this wavelength is prevented from being reflected, it will result in a negative result in terms of photocatalytic efficiency.

The photocatalytic degradation efficiencies of all TiO_2 samples are gathered in figure 7(a). The E1 sample stands out as having the lowest photocatalytic efficiency, while the AE4 sample stands out as having the highest efficiency among the samples. This means that AE4 shows the fastest degradation activity. The photocatalytic activity ranking is listed as E4 > E3 > E2 > E1 for the etching sample group and AE4 > AE3 > AE2 > AE1 for the etched/anodized sample group. It can be seen that the samples that can be considered in terms of photocatalytic efficiency are the samples that were anodized with the third and fourth solutions. Structural-colored TiO_2 coatings with photocatalytic efficiency in the range of 40 to 68% were obtained. When the literature studies are examined, it can be seen that TiO_2-based catalysts, especially those produced in powder form, exhibit very high yields [68–73]. However, it has been observed that TiO_2 catalysts produced as coatings as in our study, exhibit photocatalytic efficiency in the range of 30%–75% [74–79]. Although this efficiency is up to 83%–95% in some studies [80, 81], it is thought to be sufficient efficiency obtained for structurally colored TiO_2 coatings with two special properties.

When looking at the photocatalytic degradation variations among the anodized samples, there are various reasons for the different efficiency values [82, 83]. Crystalline lattice structure, surface morphology and optical properties can be listed as potential reasons [84, 85]. Among these reasons, the only factor that we cannot associate with the results is the crystal lattice structure. However, it can be associated with photocatalytic efficiency to surface morphology to some extent. While the fourth solution samples with high surface area with nanofiber surface morphology exhibit the highest yields, it is quite consistent that the samples etched with the first solution, which forms indentation-protrusion and micro-pores on the surface, exhibit the lowest efficiencies. However, the higher photocatalytic performance of the E3 sample with micro and nanoporous surface morphology than the nanopore E2 sample group indicates that it is a more important parameter affecting the photocatalytic efficiency. Therefore, the optical properties of the samples should be interpreted for the photocatalytic performance of the materials. High-reflectance values decrease photocatalytic reactions because the reflectance interactions cause energy loss, by coming to the surface of the material to be reflected back [86]. This explains why the nanoporous E2 sample exhibits lower yields. The advantage provided by the nanopores for the photocatalytic performance of the samples etched with the second solution has disappeared as they did not exhibit high reflectance. Therefore, it would be more appropriate to locate pPBG at higher wavelengths with lower energy in areas where photocatalytic efficiency is intended

The stability graph of the EA4 sample, which showed the best photocatalytic properties, which was carried out in 5 cycles of 150 min for each cycle, is given figure 7(b). It can be seen from this graph that there is no

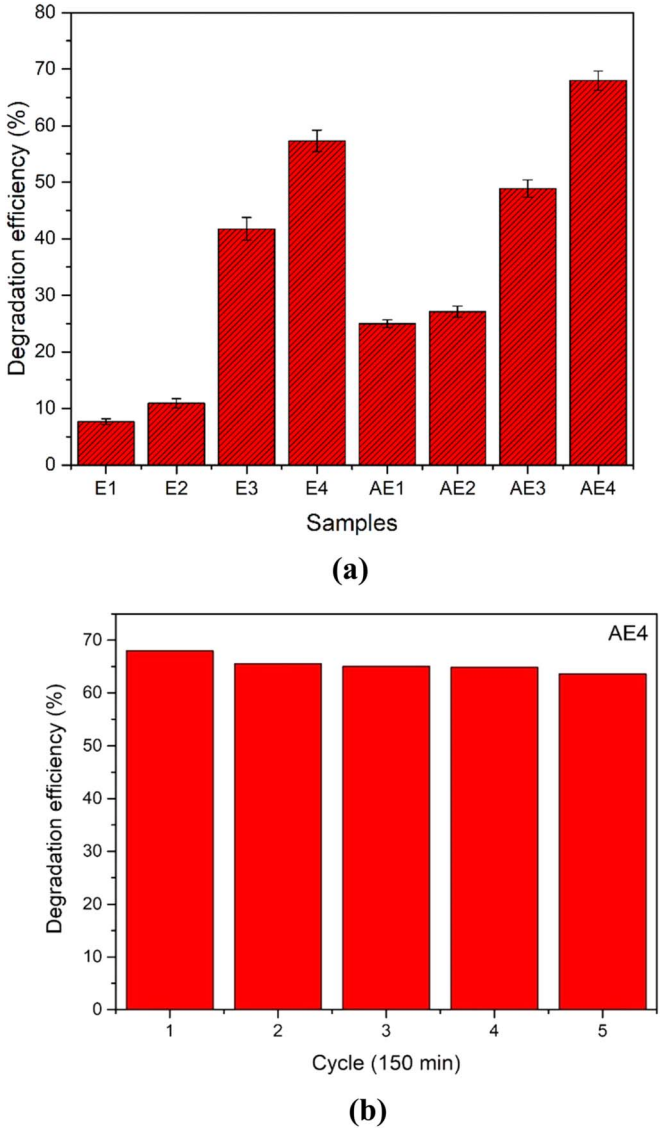

Figure 7. (a) The degradation efficiency diagram of the samples [47] and (b) the photodegradation efficiency curves of AE4 sample for 5 cycles.

significant change in photocatalytic degradation efficiency. Photocatalytic efficiency showed a decrease of about 5% after five cycles. This shows that produced samples have high photocatalytic stability.

4. Conclusions

Anatase thin films were grown successfully on Ti samples for all etching solutions. Indentation-protrusion, nanoporous, microporous, flake, and nanofiber morphologies were obtained on the surfaces. The structural color formation was observed on surfaces with almost regular indentation or porous morphology. The addition of the HF and HNO_3 chemicals to the H_2SO_4 caused the micro-pores to turn into nano-pores. Generally, the anodization process made the porous and fibrous morphologies more micro-porous. Etching by the solution containing HF provides the highest reflectance values while the KOH-based solution provides the lowest reflectance values. The structural color of formation on the titanium surfaces was explained by the FP structures, while variations were correlated with PC surface morphologies. The anodization process blue shifted the reflectance spectrum and also decreased the reflectance values of the etched samples. Generally, purple, blue, and orange colors were observed on the etched and anodized sample surfaces etched by the first ($HCl+H_2SO_4$) and second ($HF+HNO_3+H2SO_4$) solutions. The second etching solution can be suggested as an etching solution for the microstructural investigation of Titanium. The decrease in photocatalytic efficiency from the fourth solution to the first solution reveals that basic solutions provide higher photocatalytic efficiency. High-reflectance values decrease photocatalytic reactions as the reflectance interaction causes energy loss. Therefore, it

is thought that shifting the structural color to red may allow obtaining coatings with higher photocatalytic efficiency.

Acknowledgments

The preliminary version was presented orally at the '3rd International Congress on Life, Social, and Health Sciences in a Changing World' and has been published as part of its proceeding book [47].

Data availability statement

All data that support the findings of this study are included within the article (and any supplementary files).

Funding statement

We would like to thank Dokuz Eylül University for providing open access to the article with the read and publish agreement.

Author contributions

Ozan Yilmaz: Conceptualization, Investigation, Methodology, Validation, Visualization, Writing-original draft Writing-review and editing; Ramazan Dalmis: Conceptualization, Investigation, Methodology, Validation, Visualization, Writing-original draft, Writing-review and editing; Tuncay Dikici: Conceptualization, Investigation, Methodology, Visualization, Writing-review and editing; Mehmet Ebeoglugil: Conceptualization, Visualization, Writing-review and editing.

Conflict of interest

On behalf of all authors, the corresponding author states that there is no conflict of interest.

ORCID iDs

Ramazan Dalmis https://orcid.org/0000-0002-5508-2539

References

[1] Zhu H *et al* 2021 Integration of water collection and purification on cactus- and beetle-inspired eco-friendly superwettable materials *Water Res.* **206** 117759
[2] Hrudey S E 2009 Chlorination disinfection by-products, public health risk tradeoffs and me *Water Res.* **43** 2057–92
[3] Bai H W, Liu L, Liu Z Y and Sun D D 2013 Hierarchical 3D dendritic TiO_2 nanospheres building with ultralong 1D nanoribbon/wires for high performance concurrent photocatalytic membrane water purification *Water Res.* **47** 4126–38
[4] Wang D W, Mueses M A, Marquez J A C, Machuca-Martinez F, Grcic I, Moreira R P M and Li Puma G 2021 Engineering and modeling perspectives on photocatalytic reactors for water treatment *Water Res.* **202** 117421
[5] Hoffmann M R, Martin S T, Choi W Y and Bahnemann D W 1995 Environmental applications of semiconductor photocatalysis *Chem. Rev.* **95** 69–96
[6] Chong M N, Jin B, Chow C W K and Saint C 2010 Recent developments in photocatalytic water treatment technology: a review *Water Res.* **44** 2997–3027
[7] Bai H W, Liu Z Y and Sun D D 2010 Hierarchically multifunctional TiO_2 nano-thorn membrane for water purification *Chem. Commun.* **46** 6542–4
[8] Bai H W, Liu Z Y and Sun D D 2012 A hierarchically structured and multifunctional membrane for water treatment *Appl. Catal. B-Environ.* **111** 571–7
[9] Balaji U and Pradhan S K 2018 Titanium anodisation designed for surface colouration - Systemisation of parametric interaction using response surface methodology *Mater. Design.* **139** 409–18
[10] Wadhwani C, Brindis M, Kattadiyil M T, O'Brien R and Chung K H 2018 Colorizing titanium-6aluminum-4vanadium alloy using electrochemical anodization: Developing a color chart *J. Prosthet. Dent.* **119** 26–8
[11] Dalmis R, Yilmaz O and Dikici T 2021 A new concept for the eco-friendly structural colorization of anodic titania: photonic crystal structure *Colloid Surface*A **631** 127748
[12] Keskin O Y, Dalmis R, Birlik I and Azem N F A 2020 Comparison of the effect of non-metal and rare-earth element doping on structural and optical properties of CuO/TiO_2 one-dimensional photonic crystals *J. Alloy Compd.* **817** 153262
[13] Wang B, Fei G T, Wang M, Kong M G and De L 2007 Zhang, Preparation of photonic crystals made of air pores in anodic alumina *Nanotechnology* **18** 365601

[14] Mirshafieyan S S, Guo H and Guo J P 2016 Zeroth order fabry-perot resonance enabled strong light absorption in ultrathin silicon films on different metals and its application for color filters *IEEE Photonics J.* **8** 1–12
[15] Kim J, Oh H, Seo M and Lee M 2019 Generation of reflection colors from metal-insulator-metal cavity structure enabled by thickness-dependent refractive indices of metal thin film *Acs Photonics* **6** 2342–9
[16] Li Z Y, Butun S and Aydin K 2015 Large-area, lithography-free super absorbers and color filters at visible frequencies using ultrathin metallic films *Acs Photonics* **2** 183–8
[17] Kim S J, Choi H K, Lee H and Hong S H 2019 Solution-processable nanocrystal-based broadband fabry-perot absorber for reflective vivid color generation *Acs Appl. Mater. Inter.* **11** 7280–7
[18] Kurt P, Banerjee D, Cohen R E and Rubner M F 2009 Structural color via layer-by-layer deposition: layered nanoparticle arrays with near-UV and visible reflectivity bands *J. Mater. Chem.* **19** 8920–7
[19] Haque M A, Kamita G, Kurokawa T, Tsujii K and Gong J P 2010 Unidirectional alignment of lamellar bilayer in hydrogel: one-dimensional swelling, anisotropic modulus, and stress/strain tunable structural color *Adv. Mater.* **22** 5110
[20] Sato O, Kubo S and Gu Z Z 2009 Structural color films with lotus effects, superhydrophilicity, and tunable stop-bands *Accounts Chem. Res.* **42** 1–10
[21] Liu Y S, Chang Y, Ling Z Y, Hu X and Li Y 2011 Structural coloring of aluminum *Electrochem. Commun.* **13** 1336–9
[22] Dalmis R, Azem N F A, Birlik I and Celik E 2019 SiO_2/TiO_2 one-dimensional photonic crystals doped with Sm and Ce rare-earth elements for enhanced structural colors *Appl. Surf. Sci.* **475** 94–101
[23] Dalmis R, Keskin O Y, Azem N F A and Birlik I 2019 A new one-dimensional photonic crystal combination of TiO_2/CuO for structural color applications *Ceram. Int.* **45** 21333–40
[24] Dalmis R, Birlik I, Azem N F A and Celik E 2019 Modification of the sedimentation method for PMMA photonic crystal coatings *Colloid Surface*A **577** 194–201
[25] Yabu H, Nakanishi T, Hirai Y and Shimomura M 2011 Black thin layers generate strong structural colors: a biomimetic approach for creating one-dimensional (1D) photonic crystals *J. Mater. Chem.* **21** 15154–6
[26] Kolle M, Salgard-Cunha P M, Scherer M R J, Huang F M, Vukusic P, Mahajan S, Baumberg J J and Steiner U 2010 Mimicking the colourful wing scale structure of the Papilio blumei butterfly *Nat. Nanotechnol.* **5** 511–5
[27] Kushnir S E and Napolskii K S 2018 Thickness-dependent iridescence of one-dimensional photonic crystals based on anodic alumina *Mater. Design* **144** 140–50
[28] Wu S L, Liu T F, Tang B T, Li L and Zhang S F 2019 Structural color circulation in a bilayer photonic crystal by increasing the incident angle *Acs Appl. Mater. Inter.* **11** 10171–7
[29] Phillips R W and Bleikolm A F 1996 Optical coatings for document security *Appl. Optics* **35** 5529–34
[30] Ageev E I, Veiko V P, Vlasova E A, Karlagina Y Y, Krivonosov A, Moskvin M K, Odintsova G V, Pshenichnov V E, Romanov V V and Yatsuk R M 2018 Controlled nanostructures formation on stainless steel by short laser pulses for products protection against falsification *Opt. Express* **26** 2117–22
[31] Zhu X L, Yan W, Levy U, Mortensen N A and Kristensen A 2017 Resonant laser printing of structural colors on high-index dielectric metasurfaces *Sci. Adv.* **3** e1602487
[32] Arsenault A C, Puzzo D P, Manners I and Ozin G A 2007 Photonic-crystal full-colour displays *Nat. Photonics* **1** 468–72
[33] Aguirre C I, Reguera E and Stein A 2010 *Tunable Colors in Opals and Inverse Opal Photonic Crystals* **20** 2565
2011 *Adv Funct Mater* **21** 210–210
[34] Liu F F, Xiu J H, Tang B T, Zhao D F and Zhang S F 2017 Dynamic monitoring of thermally assisted assembly of colloidal crystals *J. Mater. Sci.* **52** 7883–92
[35] Li Q L, Li X L, Wang W, Lin H, Zhuang L and Xu Y 2018 Magnetic nanoparticles modified by citrate groups for magnetically responsive photonic crystals *J. Phys. Chem. Solids* **122** 278–83
[36] Ferre-Borrull J, Rahman M, Pallares J and Marsal L 2014 Tuning nanoporous anodic alumina distributed-Bragg reflectors with the number of anodization cycles and the anodization temperature *Nanoscale Res. Lett.* **9** 1–6
[37] Hu X, Ling Z Y, Chen S S and He X H 2008 Influence of light scattering on transmission spectra of photonic crystals of anodized alumina, Chinese *Phys. Lett.* **25** 3284–7
[38] Yan P, Fei G T, Shang G L, Wu B and Zhang L D 2013 Fabrication of one-dimensional alumina photonic crystals with a narrow band gap and their application to high-sensitivity sensors *J. Mater. Chem.* C **1** 1659–64
[39] Law C S, Lim S Y, Abel A D, Voelcker N H and Santos A 2018 Nanoporous anodic alumina photonic crystals for optical chemo- and biosensing: fundamentals *Advances, and Perspectives, Nanomaterials-Basel* **8**
[40] Santos A, Law C S, Lei D W C, Pereira T and Losic D 2016 Fine tuning of optical signals in nanoporous anodic alumina photonic crystals by apodized sinusoidal pulse anodisation *Nanoscale* **8** 18360–75
[41] Hu X, Pu Y J, Ling Z Y and Li Y 2009 Coloring of aluminum using photonic crystals of porous alumina with electrodeposited Ag *Opt. Mater.* **32** 382–6
[42] Ding K W, Li M, Wang C, Lin N, Wang H R, Luo Z and Duan J A 2020 Sequential evolution of colored copper surface irradiated by defocused femtosecond laser *Adv. Eng. Mater.* **22** 1901310
[43] Marien C B D, Cottineau T, Robert D and Drogui P 2016 TiO_2 nanotube arrays: influence of tube length on the photocatalytic degradation of paraquat *Appl. Catal. B-Environ.* **194** 1–6
[44] Li W J, Liang R, Hu A M, Huang Z H and Zhou Y N 2014 Generation of oxygen vacancies in visible light activated one-dimensional iodine TiO_2 photocatalysts *RSC Adv.* **4** 36959–66
[45] Oluremi O, Bukola A, Babalola J and Olubambi P A 2022 Microstructures and mechanical properties of ceramics reinforced titanium matrix fabricated by pulsed electric current sintering *Journal of Materials Research and Technology* **17** 2807–17
[46] Xie Y B and Li X Z 2006 Preparation and characterization of TiO_2/Ti film electrodes by anodization at low voltage for photoelectrocatalytic application *J. Appl. Electrochem.* **36** 663–8
[47] Yilmaz O, Ebeoglugil M F, Dalmis R and Dikici T 2021 The effect of the etching solution type on anodic TiO_2 photocatalysis, 3rd international congress on life, social, and health sciences in a changing *World, ISCYA* 234–9
[48] Tsega M and Dejene F B 2017 Influence of acidic pH on the formulation of TiO_2 nanocrystalline powders with enhanced photoluminescence property *Heliyon* **3** e00246
[49] Kar A, Smith Y R and Subramanian V 2009 Improved photocatalytic degradation of textile dye using titanium dioxide nanotubes formed over titanium wires *Environ. Sci. Technol.* **43** 3260–5
[50] Pazokifard S, Mirabedini S M, Esfandeh M and Farrokhpay S 2012 Fluoroalkylsilane treatment of TiO_2 nanoparticles in difference pH values: characterization and mechanism *Adv. Powder Technol.* **23** 428–36

[51] Demirci S, Dikici T, Tuncay M M and Kaya N 2020 A study of heating rate effect on the photocatalytic performances of ZnO powders prepared by sol-gel route: Their kinetic and thermodynamic studies *Appl. Surf. Sci.* **507** 145083
[52] Ban S, Iwaya Y, Kono H and Sato H 2006 Surface modification of titanium by etching in concentrated sulfuric acid *Dent. Mater.* **22** 1115–20
[53] Hung K Y, Lin Y C and Feng H P 2017 The effects of acid etching on the nanomorphological surface characteristics and activation energy of titanium medical materials *Materials* **10** 1164
[54] Barrera-Patino C P, Vollet J D, Teixeira-Rosa R G, Quiroz H P, Dussan A, Inada N M, Bagnato V S and Rey-Gonzalez R R 2020 Photonic effects in natural nanostructures on Morpho cypris and Greta oto butterfly wings *Sci Rep.* **10**
[55] Niu S C, Li B, Mu Z Z, Yang M, Zhang J Q, Han Z W and Ren L Q 2015 Excellent structure-based multifunction of morpho butterfly wings: a review *J. Bionic Eng.* **12** 170–89
[56] Zhang S C and Chen Y F 2015 Nanofabrication and coloration study of artificial Morpho butterfly wings with aligned lamellae layers *Sci Rep.* **5** 16637
[57] Zhao X C, Ren X J, Wang C Z, Huang B X, Ma J, Ge B, Jia Z F and Li Y C 2020 Enhancement of hydroxyapatite formation on titanium surface by alkali heat treatment combined with induction heating and acid etching *Surf Coat Tech* **399** 126173
[58] Kim C, Kendall M R, Miller M A, Long C L, Larson P R, Humphrey M B, Madden A S and Tas A C 2013 Comparison of titanium soaked in 5 M NaOH or 5 M KOH solutions *Mat Sci Eng C-Mater* **33** 327–39
[59] Wandiyanto J V, Tamanna T, Linklater D P, Truong V K, Al Kobaisi M, Baulin V A, Joudkazis S, Thissen H, Crawford R J and Ivanova E P 2020 Tunable morphological changes of asymmetric titanium nanosheets with bactericidal properties, J Colloid Interf *Sci* **560** 572–80
[60] Zhang K, Tang Y W, Meng J S, Wang G, Zhou H, Fan T X and Zhang D 2014 Polarization-sensitive color in butterfly scales: polarization conversion from ridges with reflecting elements *Opt. Express* **22** 27437–50
[61] Karambakhsh A, Afshar A, Ghahramani S and Malekinejad P 2011 Pure commercial titanium color anodizing and corrosion resistance *J. Mater. Eng. Perform.* **20** 1690–6
[62] Dalmis R, Birlik I, Azem N F A and Celik E 2020 Structurally colored silica photonic crystal coatings modified by Ce or Eu rare-earth dopants *Colloid Surface* A **603**
[63] Dalmis R, Birlik I, Azem N F A and Celik E 2021 Comparison of Sm3+ and Tb3+ dopant effects on the silica-based three-dimensional inverse opal photonic crystal coatings *J. Mater. Sci-Mater El*
[64] Hwang S K, Jeong S H, Hwang H Y, Lee O J and Lee K H 2002 Fabrication of highly ordered pore array in anodic aluminum oxide *Korean J. Chem. Eng.* **19** 467–73
[65] Saravanan R, Gupta V K, Narayanan V and Stephen A 2013 Comparative study on photocatalytic activity of ZnO prepared by different methods *J. Mol. Liq.* **181** 133–41
[66] Konstantinou I K and Albanis T A 2004 TiO_2-assisted photocatalytic degradation of azo dyes in aqueous solution: kinetic and mechanistic investigations - a review *Appl. Catal. B-Environ.* **49** 1–14
[67] Marschall R and Wang L Z 2014 Non-metal doping of transition metal oxides for visible-light photocatalysis *Catal. Today* **225** 111–35
[68] Gupta S and Tripathi M 2011 A review of TiO_2 nanoparticles *Chinese Sci. Bull* **56** 1639–57
[69] Ayati A, Ahmadpour A, Bamoharram F F, Tanhaei B, Manttari M and Sillanpaa M 2014 A review on catalytic applications of Au/TiO_2 nanoparticles in the removal of water pollutant *Chemosphere* **107** 163–74
[70] Chen P C, Chen C C and Chen S H 2017 A review on production, characterization, and photocatalytic applications of TiO_2 nanoparticles and nanotubes *Curr. Nanosci.* **13** 373–93
[71] Mustapha S, Ndamitso M M, Abdulkareem A S, Tijani J O, Shuaib D T, Ajala A O and Mohammed A K 2020 Application of TiO_2 and ZnO nanoparticles immobilized on clay in wastewater treatment: a review *Appl. Water Sci.* **10** 1–36
[72] Daghrir R, Drogui P and Robert D 2013 Modified TiO_2 for environmental photocatalytic applications: a review *Ind. Eng. Chem. Res.* **52** 3581–99
[73] Chen J R, Qiu F X, Xu W Z, Cao S S and Zhu H J 2015 Recent progress in enhancing photocatalytic efficiency of TiO_2-based materials *Appl. Catal a-Gen.* **495** 131–40
[74] Dikici T, Yurddaskal M, Yildirim S and Celik E 2018 Influence of growth parameters on the properties of TiO2 films prepared by anodic spark oxidation method and photocatalytic degradation of methylene blue *J. Aust. Ceram. Soc.* **54** 451–8
[75] Liu G Y, Xia H Y, Niu Y H, Zhao X, Zhang G T, Song L F and Chen H X 2020 Photocatalytic performance of doped TiO_2/AC coating and its UV stability research *Prog. Org. Coat.* **148** 105882
[76] Barmeh A, Nilforoushan M R and Otroj S 2019 Photocatalytic and self-cleaning properties of glazed ceramic tiles coated with TiO_2 and Al-doped TiO_2 thin films *J. Aust. Ceram. Soc.* **55** 1091–7
[77] Demirci S, Dikici T, Yurddaskal M, Gultekin S, Toparli M and Celik E 2016 Synthesis and characterization of Ag doped TiO_2 heterojunction films and their photocatalytic performances *Appl. Surf. Sci.* **390** 591–601
[78] Erol M, Dikici T, Toparli M and Celik E 2014 The effect of anodization parameters on the formation of nanoporous TiO_2 layers and their photocatalytic activities *J. Alloy Compd.* **604** 66–72
[79] Yi Z, Liu J, Wei W, Wang J and Lee S W 2008 Photocatalytic performance and microstructure of thermal-sprayed nanostructured TiO_2 coatings *Ceram. Int.* **34** 351–7
[80] Dikici T, Yurddaskal M, Demirci S and Celik E 2017 The effects of growth conditions on the surface properties and photocatalytic activities of anatase TiO_2 films prepared via electrochemical anodizing and annealing methods *J. Porous Mat.* **24** 1535–44
[81] Yurddaskal M, Dikici T, Yildirim S, Yurddaskal M, Toparli M and Celik E 2015 Fabrication and characterization of nanostructured anatase TiO_2 films prepared by electrochemical anodization and their photocatalytic properties *J. Alloy Compd.* **651** 59–71
[82] Qin J L, Cao Z G, Li H and Su Z X 2021 Formation of anodic TiO_2 nanotube arrays with ultra-small pore size *Surf. Coat. Tech.* **405** 126661
[83] Maia V A, Paschoal F M and Braga N A 2022 TiO_2 nanotubes produced by the anodization process under different parameters *J. Porous Mat.* **29** 1981–9
[84] Hou X L, Lund P D and Li Y D 2022 Controlling anodization time to monitor film thickness, phase composition and crystal orientation during anodic growth of TiO_2 nanotubes *Electrochem. Commun.* **134** 107168
[85] Devi K P, Goswami P and Chaturvedi H 2022 Fabrication of nanocrystalline TiO_2 thin films using Sol-Gel spin coating technology and investigation of its structural, morphology and optical characteristics *Appl. Surf. Sci.* **591** 153226
[86] Yamada I 2022 Fabrication of a reflective polarization wavelength filter via anodization of a Ti grating film *Appl. Optics.* **61** 5483–8